Model-free anti-swing control of complex-shaped payload with offshore floating cranes and a large number of lift wires

Zhengru Ren [a,b], Amrit Shankar Verma [a,b,c,d,*], Behfar Ataei [a,e], Karl Henning Halse [a,e], Hans Petter Hildre [a,e]

[a] Centre for Research-based Innovation of Marine Operations (SFI MOVE), Norway
[b] Department of Marine Technology, Norwegian University of Science and Technology (NTNU), NO-7491 Trondheim, Norway
[c] Faculty of Aerospace Engineering, Aerospace Manufacturing Technologies, Delft University of Technology, Delft 2629 HS, Netherlands
[d] Department of Ships and Ocean Structures, SINTEF Ocean AS, Trondheim , Norway
[e] Department of Ocean Operations and Civil Engineering, NTNU, NO-6025 Aalesund, Norway

ARTICLE INFO

ABSTRACT

Being one of the most commonly used offshore operations, offshore lifting operations become increasingly challenging due to the gradually growing size and weight of payloads. The research on automatic control in lifting operations, e.g., anti-swing control and heave compensation, only considers simple-shaped payloads, such as lumped-mass rigid points. However, the sizes and orientations of many structures cannot be neglected. To lift heavy and large-scale payloads, larger and higher cranes are required. Alternatively, it is possible to share the total loads by enhancing the number of lift wires that may limit the tension on each lift wire. However, the complicated configuration introduces significant complexity into the design of the automatic anti-swing algorithm, especially to the control allocation module. This paper performs a preliminary study on the anti-swing control of a complex-shaped suspended payload lift using a floating crane vessel and a large number of lift wires. Inspired by the knowledge of inverse dynamics and range-based localization, a general model-free anti-swing control scheme is proposed. The controller has a simple form without considering state–space equations, but it can reduce the pendular payload motion regardless of the detailed system configuration. An offshore wind turbine tower–nacelle–rotor preassembly installation using floating crane vessel is adopted as a case study to verify the performance of the proposed control strategy.

1. Introduction

The sizes and weights of offshore structures have grown dramatically in the recent decades. For example, the height of the newly launched Haliade-X 12 MW wind turbine reaches 260 m, and its nacelle and rotor reaches to 825 tons. Though the benefits of extremely large structures are welcomed by industry and researchers, the trend engenders new challenges with the offshore operations, such as lifting and mating operations. Lifting is one of the most commonly used offshore operations. With increasing installation heights and increasing weights of the payloads, higher and more powerful cranes are required to accomplish the specific offshore operations. For some complex projects, only a small range of vessels is capable of executing the tasks, which may limit the development of the relevant industry.

For a lifting operation using a floating crane, the suspended payload oscillates due to the floating vessel motion and exposure to wind. The payload and vessel are coupled through the lift wires and cranes. The first- and second-order wave-induced motions are mainly influenced by the sea states, which can be estimated by optimization methods (Ren et al., 2021a) and neural networks (Cheng et al., 2020), but impossible to be fully canceled. To reduce the pendular motions of a suspended payload, anti-swing control is studied by controlling cranes and the corresponding winch servo motors. Complex control algorithms have been applied to anti-sway control for a lumped-mass payload, such as PID control (Solihin et al., 2009), LQR control (Adeli et al., 2011), robust adaptive control (Qian et al., 2019), neural adaptive control (Yang et al., 2019; Kim et al., 2020), and fuzzy sliding mode control (Ngo et al., 2017).

In previous studies, the lift wire characteristics, motions of the payload and vessel, number of lift wires, and environmental loads are

simplified. First, the elongations of the lift wires are disregarded, or the linear-spring model with constant stiffness is adopted. However, a practical lift wire can only provide positive tension, and its wire elongation influences the payload motion. The complexity of the lift wire characteristics introduces difficulties in the design process. Furthermore, control designs are based on simplified models. The dynamics of the payload are modeled as a 2-degree-of-freedom (DOF) or 3-DOF lumped mass by neglecting the minor DOFs and using Lagrangian mechanics (Neupert et al., 2008; Yang et al., 2019; Qian et al., 2019; Ngo et al., 2017) and Newton–Euler methods (Ren et al., 2019a; Chu et al., 2015; Ku et al., 2013). The control performance can be inferior due to poor modeling, and the influence caused by the unmodeled DOFs is not controllable. Third, only one lift wire is considered in most research for the sake of simplification. Extra lift wires complicate the control allocation algorithm. Finally, the environmental loads are neglected since the loads are normally much lower than the payload weight and the pendular motion is the main concern. Nevertheless, the wind loads acting on the complex-shaped payload may have a considerable influence on the system.

Instead of using larger equipment, it is possible to achieve the same performance with a combination of low-capability ones, resulting in a lower installation height and lower tension on each lift wire. However, the control algorithm can be quite complex if the elongation is considered and the lift wires are arranged in 3D space and no longer can be assumed to only act in the vertical direction.

The problem of offshore wind turbine installation arises with the global explosive growth in wind energy (Jiang et al., 2017; Ren et al., 2021c). There are a number of installation strategies according to the onshore preassembly level (Vis and Ursavas, 2016). To further reduce the electricity price of offshore wind, improve installation efficiency, and ensure operation safety, much research about monopile foundation installation (Acero et al., 2016), single blade installation (Verma et al., 2019; Ren et al., 2019b, 2018a), rotor–nacelle–rotor preassembly installation (Ren et al., 2021b), and loading and unloading operations (Kjelland and Hansen, 2015) has been conducted. Compared with the separate-part strategy, the rotor–nacelle–rotor preassembly installation reduces offshore installation time due to the lower number of offshore lifting operations.

In this paper, we propose an anti-swing control strategy to the lifting operation with a complex-shaped payload and multiple lift wires. The main advantages of the proposed controller are the simple control design without the employment of complex state–space models and control allocation, model-free characteristic, and the freedom from building the control allocation matrix, and reduced crane heights. The winch servo motors are controlled. To the best of the authors' knowledge, the methodology is first adopted herein to achieve automatic floating lifting control.

The paper is organized as follows. In Section 2, the system configuration is illustrated, and the control problem is formulated. In addition, the challenges of lift wires are discussed. Section 3 presents the proposed novel control scheme. A wind turbine tower–nacelle–rotor preassembly is taken as an example of payload, and the control scheme is verified by simulations in Section 4. The paper is summarized in Section 5.

2. Problem formulation

In this section, a general lifting problem using a floating vessel is presented. A complex-shaped payload is lifted by the cranes mounted on a floating crane vessel through lift wires; see Fig. 1. The second-order wave drift force are compensated by a dynamic positioning (DP) system, resulting the vessel's mean horizontal position and heading are stabilized. The details about the DP system are neglected since it is not the main focus of the present paper. However, the first-order wave-induced surge, sway, and yaw as well as the roll, pitch, and heave motions are not controlled, resulting in payload motions.

For a large-scale payload, the weight is very likely to be too high to be lifted by a single lift wire. Hence, an increasing number of lift wires are necessary to share the total loads and limit the load acting on each lift wire. By doing this, it is possible to accomplish controlled heavy lifting with a large number of lift wires. Instead of connecting to the top of the payload, lift wires can connect the payload at p_c. Hence, the positions of the crane tips or pulleys on the crane booms p_b can be lower. Suppose that there are M groups of lift wires and that the group index is denoted by i, $i \in \{1, \ldots, M\}$. In the ith group, the number of lift wires is N_i, and the index of a lift wire is j ($j \in \{1, \ldots, N_i\}$). The length of the jth lift wire in ith group without elongation is l_{ij}. The payload is assumed to be a rigid body.

The proposed lifting configuration introduces significant complexity into the control design. Hereafter in this section, the challenges and control problem are stated.

2.1. Coordinate systems

The objects of interest are the vessel and payload. Hence, three right-handed coordinate systems are adopted in the present paper as follows:

- Local north-east-down (NED) reference frame $\{n\}$: The origin O_n is fixed at the free water surface. The directions of the x-, y-, and z-axes point to the north, to the east, and downward, respectively.
- Vessel body-fixed reference frame $\{v\}$: The origin O_v is placed at the vessel's centers of gravity (COG). The x^v-, y^v-, and z^v-axes are from the aft to the bow, from the portside to starboard, and downward, respectively.
- Payload body-fixed reference frame $\{b\}$: It is defined similarly to $\{v\}$ by placing the origin at the payload's COG. The axes can be defined according to the specific configuration. The Euler angle vector of the payload is defined as $\Phi = [\phi, \theta, \psi]^\top$.

The vessel orientations about the x^v-, y^v-, and z^v-axes are not introduced since they are not actively controlled hereafter. Superscripts denote the corresponding reference frames for vectors.

2.2. Challenges of a complex lifting control system

The automatic lifting problems are challenging due to the high number of DOFs, nonlinearities caused by lifting wires, heavy payload, and large number of lift wires.

2.2.1. Complex-shaped payload and number of lift wires

In addition to the rigid-point payloads with concentrated gravity, a payload can be complex-shaped in many practical applications. To control its motion and realize specific operations, e.g., stabilizing or smoothly following the planned trajectory, 6-DOF payload control is necessary for specific scenarios (Niu et al., 2018). For example, the orientations of the wind turbine blade should be controlled in its mating stage to ensure the guide pin at the root of the blade faces the hub mating flange. The high number of states is a challenge to the control design. In addition, the payload COG is difficult to be accurately determined, and the rotation matrices complicate the control design.

Operating the cranes is a slow and energy-consuming task. Hence, the crane motion is too slow to be controlled. When there are many cranes, the instant power consumption challenges the power generation system, resulting in the risk of a blackout.

2.2.2. Nonlinearities caused by lifting wires

In previous studies, the payload is assumed to be lightweight, and the dynamic tension on and elongation of the lift wire are neglected. The control inputs are normally forces acting on the lift wires or the moment acting on the crane and winch servo motors. Nevertheless, wire elongations in the lifting process of heavy offshore structures are of importance. High-fidelity modeling of lift wires can include a linear tensile spring with a damper and provide tension force with positive
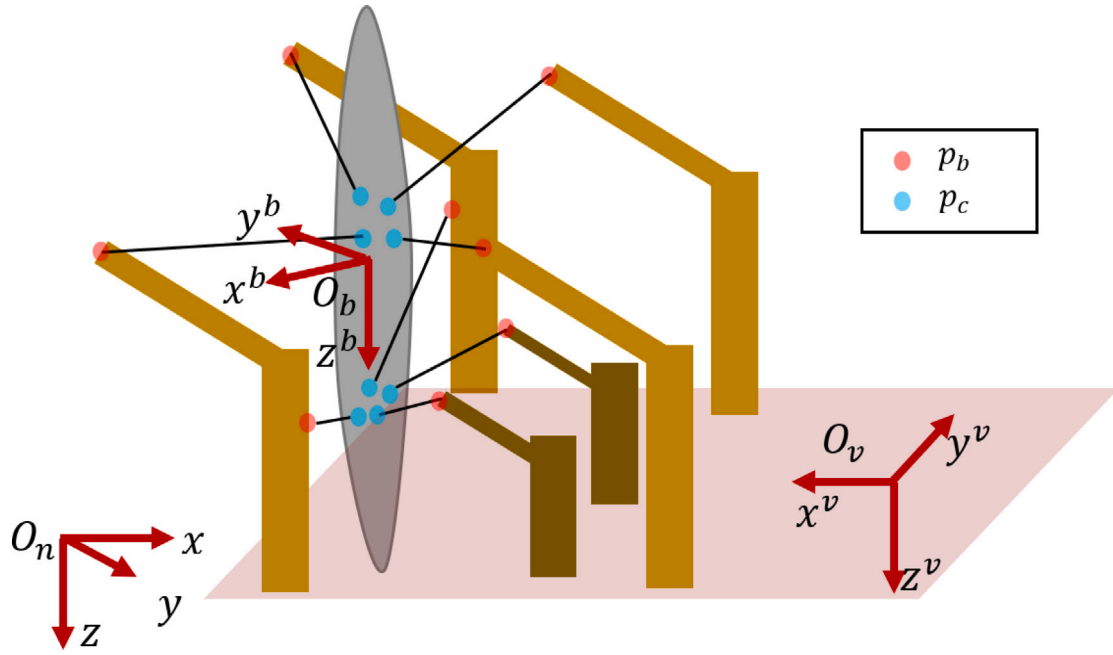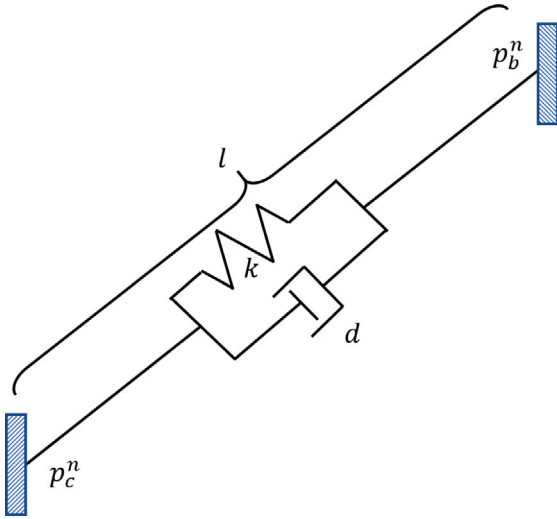
Fig. 1. Diagram of the complex lifting scenario.

Fig. 2. Diagram of a lift wire. The subscript ij is removed to provide general notations.

elongation, as shown in Fig. 2. No restoring force is provided when the wire is loose. The model is given by

$$T_{ij} = \max\left\{ k_{ij}\left(|p_{b,ij}^n - p_{c,ij}^n| - l_{ij}\right) - d_{ij}\left(\frac{d}{dt}|p_{b,ij}^n - p_{c,ij}^n| - \dot{l}_{ij}\right), 0 \right\}, \quad (1)$$

where the subscript ij denotes the index of the specific lift wire, $T \in \mathbb{R}$ denotes the tension, and $k \in \mathbb{R}$ and $d \in \mathbb{R}$ are the stiffness and damping coefficients, respectively. The tension force is influenced by the positions of the connecting point $p_{c,ij}^n \in \mathbb{R}^3$ and base point $p_{b,ij}^n \in \mathbb{R}^3$ in the global coordinate frame. Note that the wire line model in Eq. (1) is different from a mass–damping–spring system where the damper works to reduce the motion and the direction of the damping force is opposite to velocity. The damper in the proposed cable model works to reduce the tension, that means its direction is opposite to the relative elongation changing rate.

However, the involvement of lift wires greatly increases the complexity in control design. Lift wires introduce input nonlinearities due

to the discontinuous tension–elongation relation, the force decomposition caused by its inclination, coordinate transformation, and varying stiffness.

First, a wire rope can only provide nonnegative tension. The tension–elongation discontinuity occurs when the elongation is zero. Unlike other widely known input nonlinearities such as the deadzone and saturation, negative control input is impossible to realize using wire ropes. Typical robust and adaptive control approaches cannot handle such complexity. Moreover, the stiffness k relates to the length (Velinsky, 1985). It is normally assumed to be constant when the length change is not remarkable.

Second, the three-dimensional relative position between both ends of a wire makes the force decomposition tedious. The control allocation matrix is expressed by a group of three inclination angles or in a vector form using the relative displacement, i.e.,

$$f_{c,ij}^n = T_{ij}\frac{p_{b,ij}^n - p_{c,ij}^n}{|p_{b,ij}^n - p_{c,ij}^n|} \text{ or } f_{c,ij}^n = R(\Phi_{ij})[0,0,T_{ij}]^\top, \quad (2)$$

where red f_c^n denotes the force acting at the connecting point in $\{n\}$, $R(\cdot) \in \mathbb{R}^{3\times3}$ is a rotation matrix and $\Phi_{ij} \in \mathbb{R}^3$ is a vector of Euler angles representing the ij-th wire inclination in $\{n\}$. The rotation matrices change with the time-varying p_b and p_c resulting from the moving vessel and payload. This provokes the difficulty of linearization and the derivative of the control allocation matrix. The complexity increases with the number of lift wires.

Third, the coordinate transformation between $\{n\}$ and $\{b\}$ complicates the state equation. The tension forces should be allocated into the total restoring force and moment in the same reference frame by adopting another rotation matrix $R(\Phi)$.

2.3. Problem statement

Without loss of generality, this study, unlike previous studies, considers the lifting control in an extremely complex scenario, i.e., antiswing control of a complex-shaped 6-DOF payload using a floating vessel using a significant number of lift wires. Only winches are controlled, while the cranes are fixed. Therefore, attempts are made to design a general control scheme for the proposed complex lifting configuration with a simple form that overcomes the abovementioned difficulties.
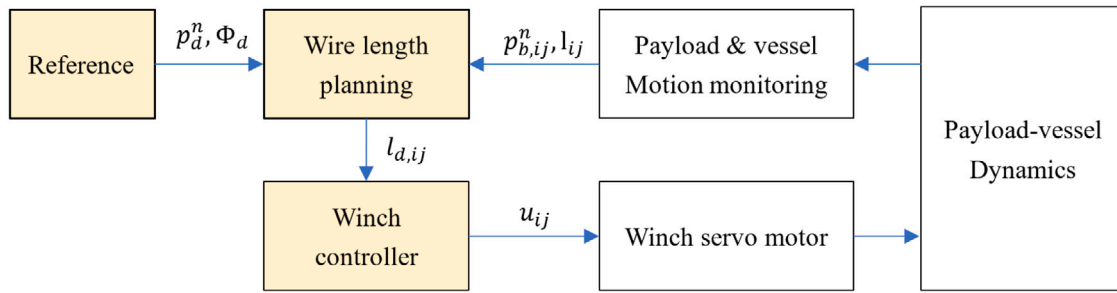
Fig. 3. Overview of the proposed control system.

In the proposed control strategy, the cranes are considered to be static and rigid. The lift wires are distributed in a dispersed manner. The position of the payload is likely to move by gravity when all lift wires are placed on one side of the payload. According to the separation principle, the observers are assumed to be already developed; i.e., the real-time positions and orientations of the vessel and payload are assumed to be known.

The control inputs are the winch servo motors. The motor dynamics is simulated by a lowpass filter. The winch model is given by

$$\dot{l}_{ij} = r_{ij} w_{ij}, \tag{3a}$$

$$\dot{w}_{ij} = -\Gamma_{ij} w_{ij} + u_{ij}, \tag{3b}$$

where r is the radius of the winch servo motor, w is the winch rotation speed, Γ is a coefficient for the lowpass filter, and u is the control input.

The object of this paper is to develop a controller to stabilize the suspended payload by controlling control input u, i.e., the position of concern p_0^n follows a slow-varying desired position $p_d(t)$ and orientation $\Theta_d(t)$, which are decided by the installation plan and real-time vessel position and heading. Specifically, we assume that p_d and Θ_d are constant.

3. Control design

3.1. System overview

According to the knowledge on localization, the position of a node is known in three-dimensional space if the distances between the unknown node with at least four landmark points with known positions are measured (Zekavat and Buehrer, 2011; Gustafsson, 2010). We assume that all lift wires are tight with positive tension. Hence, if a payload is lifted by at least four lift wires, on which the connecting points are closed, the position of the connecting point ($p_{c,i}^n$) is easily calculated when the lengths of the lift wires ($l_{i1}, \ldots, l_{i4}$) and the positions of their base ends ($p_{b,i1}^n, \ldots, p_{b,i4}^n$) are known. Additionally, the translational motion and rotation of the entire payload are determined if the positions of two connecting points on a payload ($p_{c,1}^n, p_{c,2}^n$) are controlled.

Inspired by the abovementioned knowledge, the idea of the proposed control law is to use reverse thinking of the theories. The position of a connecting point ($p_{c,i}^n$) can be determined by changing the length of at least four lift wires (l_{ij}). Therefore, at least two groups of lift wires are required, i.e., $i \geq 2$, in which the connecting points on the payload should be closed. In practical applications, a higher number of lift wires can be employed to limit the tension acting on each wire.

The ith mean connecting point position is

$$p_{c,i}^n = \frac{1}{N_i} \sum_{j=1}^{N_i} p_{c,ij}^n. \tag{4}$$

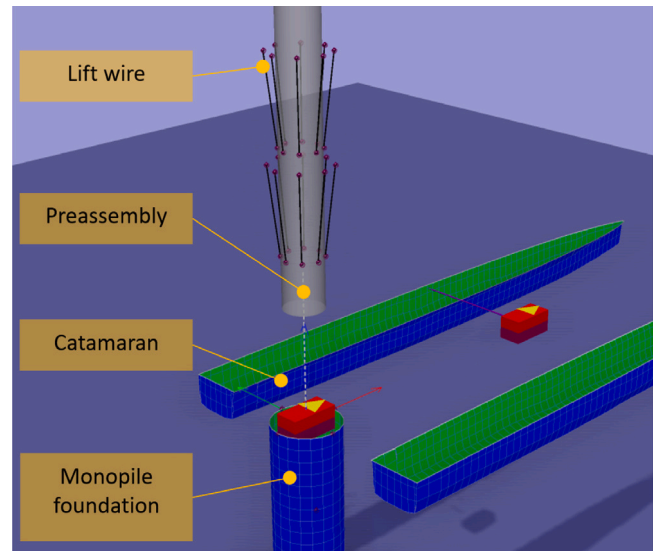The control strategy is carried out by assuming the following assumptions hold.

Fig. 4. Configuration of the OWT preassembly installation in the case study.

- The lengths of lift wires without axial elongation are known and considered as range measurements.
- The lift wire elongations are always nonnegative and small compared with their length due to the high stiffness.
- The connecting points of a group of lift wires on the payload are closed.
- The positions and orientations of the vessel and crane booms are well estimated by sensors and observer. The observer design is neglected.
- The flexibilities of the installation vessel and cranes are neglected.

The system overview is presented in Fig. 3. The measurement system detects the position and orientation of both the payload and the vessel. The reference module outputs the desired trajectory for the controller. Based on the real-time motions and desired trajectory, the wire length planning module calculates the desired wire lengths. The winch controller controls the winch servo motors to change the wire lengths.

The lift wire configuration influences the system performance. An improper arrangement may introduce instability problems and degrade the control performance. Note that a small elongation may introduce a wide range of motion to the connection point. The trend is more remarkable when the lift wires are horizontal. In addition, the payload may collapse or skew due to the improper selection of connecting points. The system configuration also influences the loads acting on the lift wires. A specific group of lift wires may contribute more than other groups, resulting in a less efficient usage of the other groups of lift wires. Consequently, some lift wires will be loose, while the others will be tight. Pretension should be applied carefully since there does not
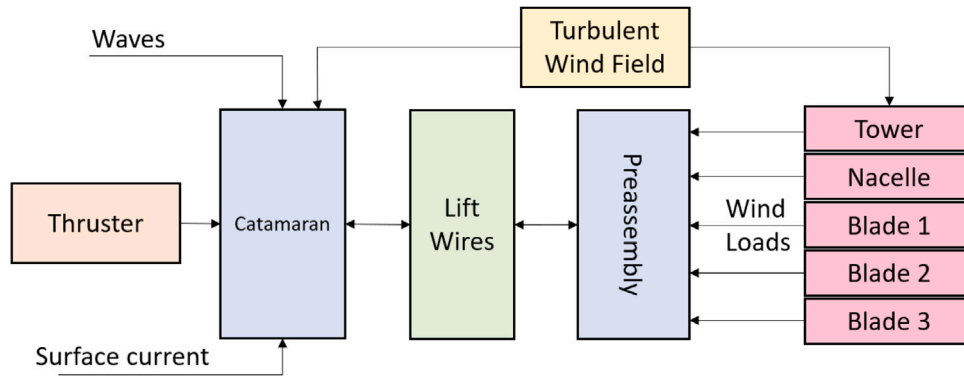
Fig. 5. Block diagram of the wind turbine preassembly system.

Table 1
Selected parameters in the simulations..

Parameter	Unit	Value
Catamaran length overall	m	144
Catamaran molded breadth	m	60
Catamaran draft	m	8.0
Displacement mass of the catamaran	tonnes	18502.9
OWT rated power	mW	10
Tower mass	tonnes	628.46
Tower height	m	115
Nacelle mass	tonnes	446.04
Blade length	m	86.366
Blade mass	tonnes	41.56
Preassembly weight	tonnes	1199.2
Position of tower bottom center in $\{b\}$ (p_0^b)	m	$[0, 0.15, 81.5]^\top$
Number of lift wires in group 1	–	8
Stiffness of lift wires in group 1	N/s	3.82e7
Damping ratio of lift wires in group 1	%	1
Number of lift wires in group 2	–	8
Stiffness of lift wires in group 2	N/s	6.44e7
Damping ratio of lift wires in group 2	%	1
Positions of the connecting points $(p_{c,1j}^b)$	m	$\begin{bmatrix} 2 & 1.41 & 0 & -1.41 & -2 & -1.41 & 0 & 1.41 \\ 0 & 1.41 & 2 & 1.41 & 0 & -1.41 & -2 & -1.41 \\ -10 & -10 & -10 & -10 & -10 & -10 & -10 & -10 \end{bmatrix}$
Positions of the connecting points $(p_{c,2j}^b)$	m	$\begin{bmatrix} 2 & 1.41 & 0 & -1.41 & -2 & -1.41 & 0 & 1.41 \\ 0 & 1.41 & 2 & 1.41 & 0 & -1.41 & -2 & -1.41 \\ 40 & 40 & 40 & 40 & 40 & 40 & 40 & 40 \end{bmatrix}$
Positions of the base points $(p_{b,1j}^v)$	m	$\begin{bmatrix} 70 & 67.07 & 60 & 52.93 & 50 & 52.93 & 60 & 67.07 \\ 0 & 7.07 & 10 & 7.07 & 0 & -7.07 & -10 & -7.07 \\ -110 & -110 & -110 & -110 & -110 & -110 & -110 & -110 \end{bmatrix}$
Positions of the base points $(p_{b,2j}^v)$	m	$\begin{bmatrix} 2 & 1.41 & 0 & -1.41 & -2 & -1.41 & 0 & 1.41 \\ 0 & 1.41 & 2 & 1.41 & 0 & -1.41 & -2 & -1.41 \\ -50 & -50 & -50 & -50 & -50 & -50 & -50 & -50 \end{bmatrix}$

exist any constraint in the vertical upward direction and the pretension may lift the payload to another equilibrium position. The configuration will be discussed in future publications. For the sake of simplification, the system configuration is assumed to be reasonable.

3.2. Wire length planning

Stabilization is only a part of the lifting operation. The desired position of the ijth connection point is given by

$$p_{cd,ij}^n(t) = p_d^n + R(\Phi_d)(p_{c,ij}^b - p_0^b) - K_i \int_0^t (p_0^n(\tau) - p_d^n(\tau)) d\tau, \tag{5}$$

where p_0^b and p_0^n are the positions of the concerned point in $\{b\}$ and $\{n\}$, respectively, and $K_i \in \mathbb{R}^{3\times 3}$ is a positive diagonal matrix to be tuned. According to coordinate transformation, the position of the ijth connecting point in $\{n\}$ is $p_d^n + R(\Phi_d)(p_{c,ij}^b - p_0^b)$. The term $-K_i \int (p_0^n(\tau) - p_d^n(\tau)) d\tau$ is used to compensate for the bias caused by the wire elongation. It is similar to an integral controller, where the control gains are the coefficients in matrix K_i.

The desired length of the lift wire is given by

$$l_{d,ij}(t) = |p_{cd,ij}^n(t) - p_{b,ij}^n(t)|. \tag{6}$$

3.3. Winch control

The length of lift wire is controlled by its corresponding winch. The winch velocity is

$$u_{ij} = \frac{k_p}{r_{ij}}(l_{ij} - l_{d,ij}), \tag{7}$$

where $k_p > 0$ is a control gain.

3.4. Summary

According to inverse dynamics, a model-free control scheme of complex offshore anti-swing control using a large number of lift wires is proposed. There should be at least two groups of lift wires and at least four lift wires in each group. The largest advantage is the
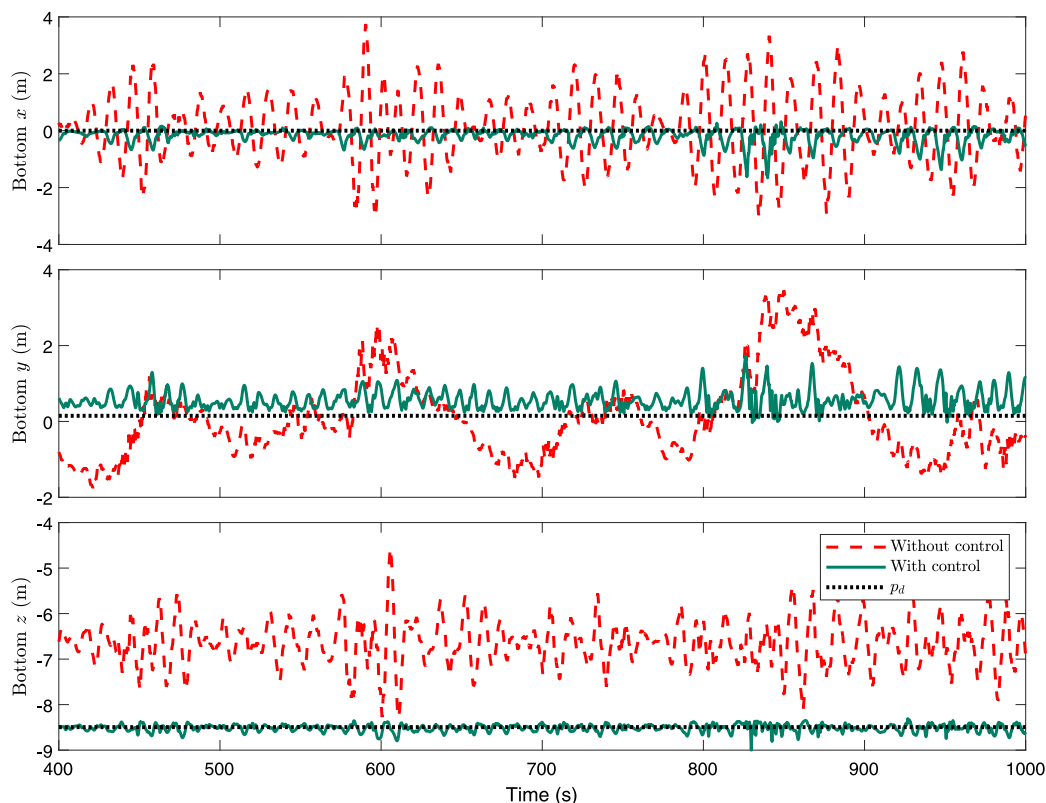
Fig. 6. Motions at the tower bottom center in 400–1000 s in EC1.

simple control design which does not consider the exact state–space model. The planning function (5) and the control law (7) only rely on real-time motion measurements of the floating cranes and suspended payload. Besides, the complicated three-dimensional control allocation is avoided.

4. Case study: tower–nacelle–rotor preassembly installation using a catamaran vessel

4.1. System description

Hereafter, an offshore wind turbine (OWT) preassembly installation is adopted as the research scenario. The superstructures, including tower, nacelle, and rotor, are preassembled onshore and carried to the installation site. It is assumed that the monopile foundation has been installed. The installation is accomplished with only one lift operation, resulting in a higher installation efficiency. A newly developed idea is to lift the preassembly using several groups of lift wires, which connects at the tower of the preassembly; see Fig. 4. The lift wires connect with their corresponding winches through the pulleys fixed on the vessel body-fixed reference frame. For the OWT preassembly installation scenario, the motion of the suspended preassembly is dominated by the floating vessel. The influence of the turbulent wind field is limited. The relative position between the tower bottom center and foundation top center affects the operational successful rate, and the corresponding relative velocity influences the impact force. In addition, the motion amplitude of monopile foundation is small compared with the assembly bottom motion. Therefore, the target is to achieve a anti-swing control which stabilizes the payload in the air at the tower bottom center and maintains the orientation such that it achieves a smooth mating operation.

Table 2
Environmental conditions in the simulations.

EC	H_s (m)	T_p (s)	β_{wave} (deg)	U_w (m/s)	TI (%)	β_{wind} (deg)
1	2.2	11.5	−23.6	3.3	17.8	−15.5
2	1.5	7.6	36.4	3.5	0.3	15.8
3	1.6	15.5	−3.4	3.5	18.3	−17.8
4	1.0	9.5	38.5	11.8	10.0	14.5
5	1.1	14.1	60.5	5.6	17.5	33.9
6	2.2	9.5	5.3	8.5	5.4	13.5
7	2.1	10.5	−32.3	4.7	18.8	−5.7
8	1.7	15.9	−34.8	11.6	18.4	−11.9
9	0.9	6.7	2.1	2.2	18.5	−22.6
10	0.9	11.9	9.2	7.5	1.2	−16.6
11	1.2	11.4	30.0	2.3	4.0	33.9
12	1.1	8.4	5.5	9.8	16.9	34.2
13	0.4	13.9	38.6	8.8	20.2	28.8
14	0.8	10.5	46.8	11.6	11.0	34.7
15	1.4	14.5	10.8	8.6	18.8	18.4
16	2.3	12.1	4.8	6.2	19.7	27.7
17	0.8	8.4	5.1	8.1	13.2	33.8
18	0.6	13.6	−2.6	6.2	4.3	−30.5
19	0.9	10.0	−15.7	4.1	23.6	7.0
20	1.0	7.9	−21.8	7.2	12.6	−32.1

4.2. Simulation overview

An overview of the simulation model is presented in Fig. 5. Interested readers can find the modeling details for different modules in Ren et al. (2018b). The catamaran and OWT assembly are modeled with 6-DOF rigid-body dynamics. The Newton–Euler mechanism is applied. The rigid bodies are interconnected through the reacting forces and torques. The accelerations are calculated according to Newton's second law by the sum of external loads. The monopile foundation and catamaran vessel are exposed to current, waves, and wind. The influence of the current is the relative velocity. The wave-induced loads, including the first- and second-order order wave loads, are simulated with the
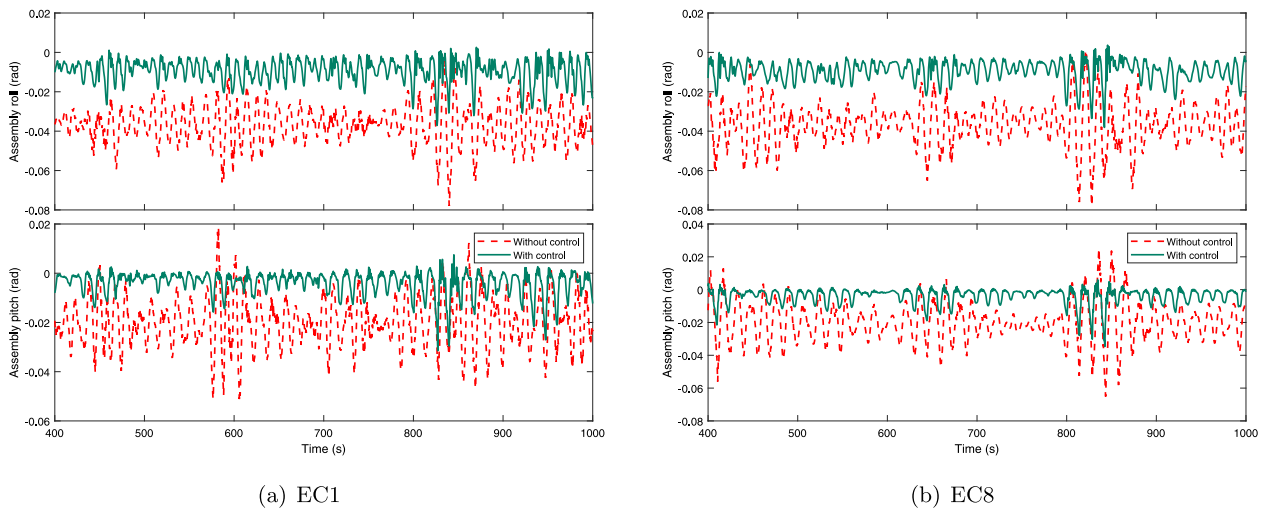
(a) EC1　　　　　　　　　　　　　　　　　(b) EC8

Fig. 7. Inclinations of the suspended assembly in 400–1000 s in EC1 and EC8.
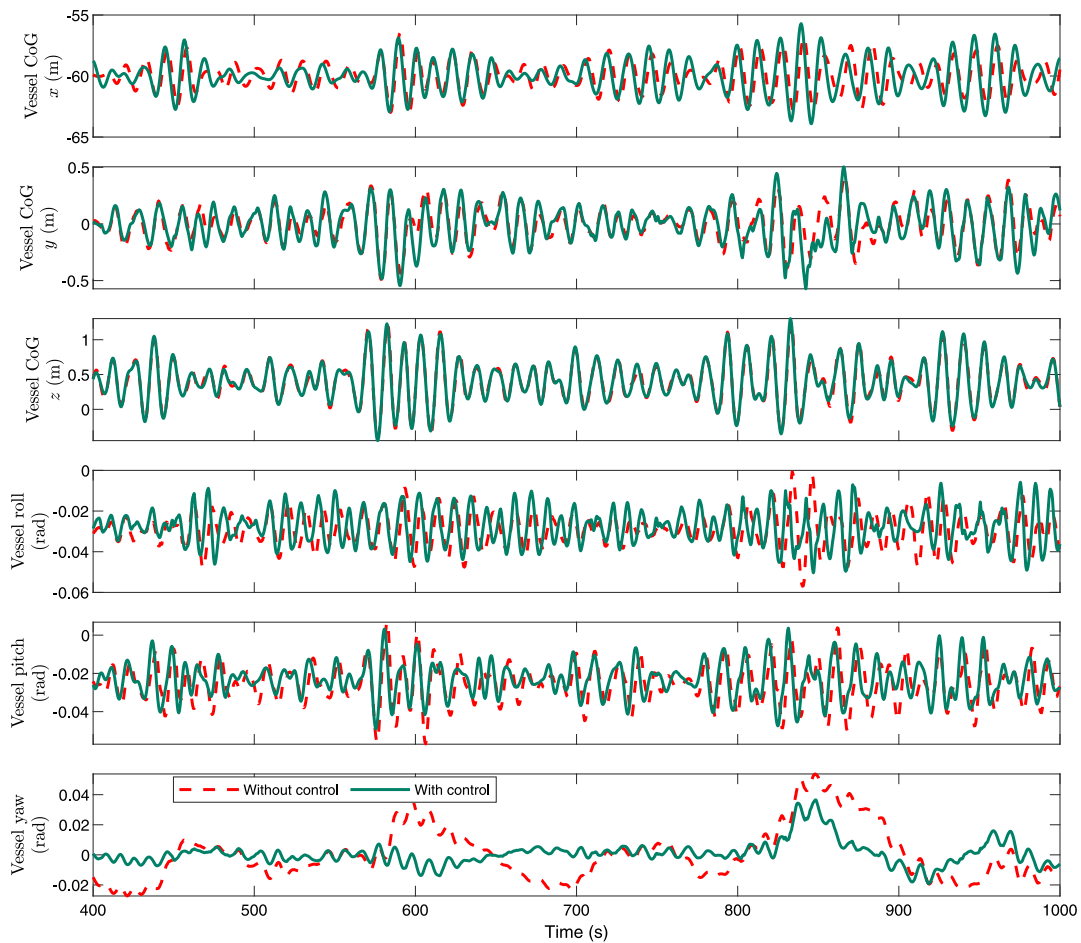

Fig. 8. Vessel motions 1 in 400–1000 s (EC 1).

force response amplitude operator (RAOs). The memory effects are simulated by several transfer functions. The hydrodynamic parameters of the catamaran are received from WAMIT. The vessel hydrodynamic model can be tuned by onboard measurements (Han et al., 2021).

The assembly is lifted by a number of lift wires, which are connected to fixed points on the vessel. Only wind-induced loads need to be considered during the modeling process. The 3D turbulent wind field is simulated using Kaimal spectrum. A turbulence box is generated
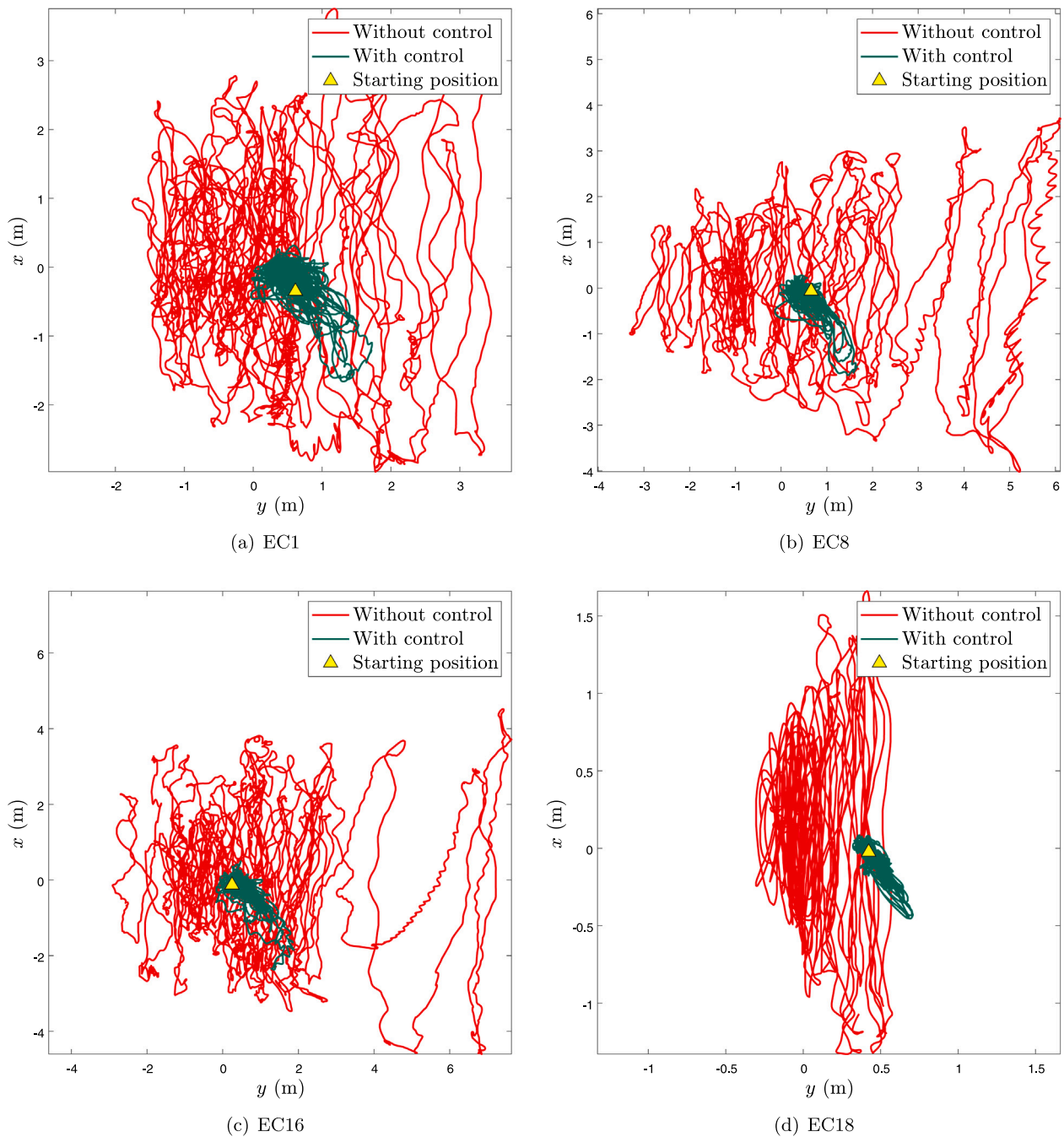
(a) EC1

(b) EC8

(c) EC16

(d) EC18

Fig. 9. The trajectories of the tower bottom in the horizontal plane.

before the simulation starts. According to Taylor's frozen turbulence hypothesis, the box is moving along its longitudinal direction with the mean wind speed. The mean wind speed, turbulence intensity TI, seed, and box size can be controlled. Specific lift and drag coefficients for the OWT components are read from a DTU 10 MW reference wind turbine (Bak et al., 2013; Tang et al., 2021). The cross-flow principle is adopted to calculate the wind-induced loads. The superposition of the aerodynamic loads acting on the tower, nacelle, and blades are exerted at the center of gravity of the OWT assembly. The coupled payload-vessel responses are considered.

The system is modeled with the MarIn toolbox (Ren et al., 2018b). In the simulations, there are 2 groups of lift wires and 8 wires in each group, i.e., $M = 2$ and $N_1 = N_2 = 8$. In total, there are 16 lift wires. The system parameters are tabulated in Table 1. The connection points are distributed on a circle with a radius of 2 m, and the base points

are distributed on a circle with a radius of 10 m. The configuration of the connecting points is a very general and complex problem, which is probably different from design to design. Besides the position of the payload COG, it depends on the wire properties, winch capacities, payload shape, etc. Therefore, a feasible configuration is selected in this paper, and it is assumed that the configuration manages to lift the payload to give a general explanation of the proposed control scheme. The number of lift wire in a group should be equal to or larger than 4. However, to limit the loads acting on each lift wire, a larger number of lift wires should be used according to the practical situation. The horizontal position of the initial assembly COG is 60 m from the vessel COG near the aft. The wind-wave misalignment is less than 30 deg.

Monte Carlo simulations are conducted to evaluate the effectiveness of the proposed control strategy in a total of 20 simulations in random environmental conditions (ECs) listed in Table 2. The environmental
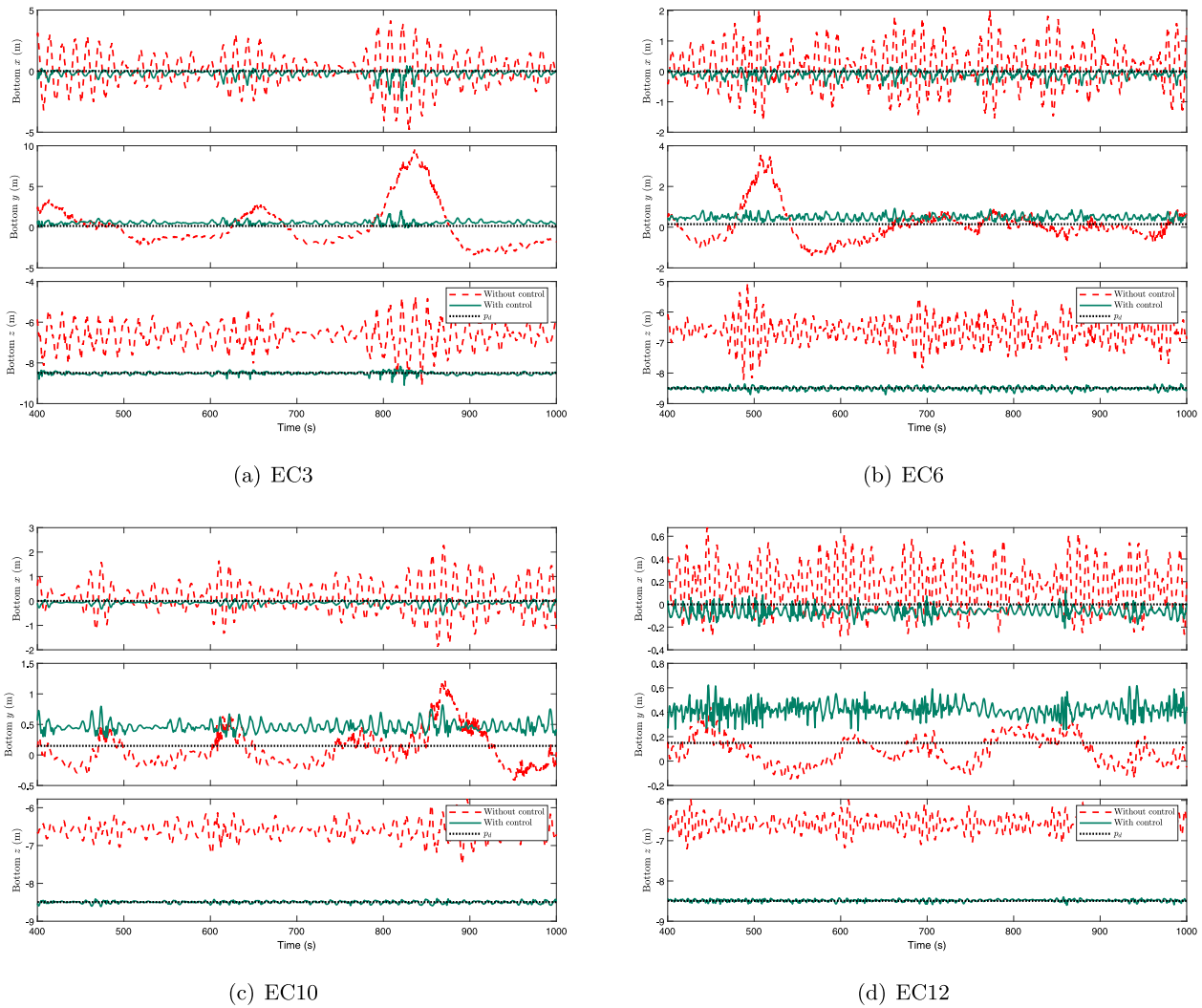
(a) EC3

(b) EC6

(c) EC10

(d) EC12

Fig. 10. Motions at the tower bottom center in some example ECs.

parameters include the significant wave height H_s, wave period T_p, wave direction β_{wave}, mean wind speed U_w, turbulence intensity TI, and wind direction β_{wind}. The wind-wave misalignment is considered. The seeds are randomly generated.

Anti-swing control is a foundation of advanced operations. Both the passive scheme without control and the active scheme with the proposed control law are simulated. In addition, the influence of the wind field is investigated. Standard derivation (STD) of the position at the tower bottom center is employed as the criteria to evaluate the system performance. Since the STD of the position is always proportional to the STD of the velocity and motion maxima, it affects both the success rate and impact force of an operation (Jiang et al., 2018; Verma et al., 2019). The simulations last for 1300 s. The initial 300 s are removed to avoid the startup effects.

4.3. Simulation results and discussion

The time-domain simulation results are presented in Figs. 6–10. Only the time-domain motions from 400 to 1000 s are plotted to avoid crowding up. The motions of the tower bottom is greatly reduced by the proposed controller; see Fig. 9. In the scenario without control, the mean wind-induced load causes a bias in the inclination. The proposed control scheme manages to regulate both the amplitude and bias in the inclinations of the suspended assembly; see Fig. 7. In addition, the reaction forces in wires slightly influences the vessel motion.

In different sea states, the STDs of the tower bottom motion are effectively reduced, approximately 70% (see Table 3 and Fig. 13). In some sea states, the specific motion reduction is not significant, e.g., y-motion in ECs 2 and 17. It is noted that the motions in the corresponding axis are quite limited. The corresponding scenarios are thus not challenging. Hence, the proposed control scheme can significantly improve the payload motion induced by the vessel motion and wind loads.

The spectra of tower bottom motions using fast Fourier transform (FFT) in x-y plane is presented in Fig. 11. The magnitudes of the peaks are well reduced by the proposed control design.

In the bar plots in Fig. 12, the STDs and maximum motion ranges are both improved by the proposed control scheme. Since the waves influence the vessel motion and the wave-induced vessel motion is of primary importance to the payload motion in the scenarios without control inputs. It is noticed that the wind turbulence field only generates minor effects to the payload motion.

At the current stage, the pendular motion is impossible to be totally canceled by the proposed controller. First, the control delay effects are unavoidable due to the motor inertia and delay caused by observers. In addition, the connection points are close but not at the same position. Hence, the motion p_i^n is restricted but not totally canceled. The system performance can be improved when the connection points are close enough; however, the practical applications is difficult in most offshore installation scenarios. Furthermore, the positions of the connecting
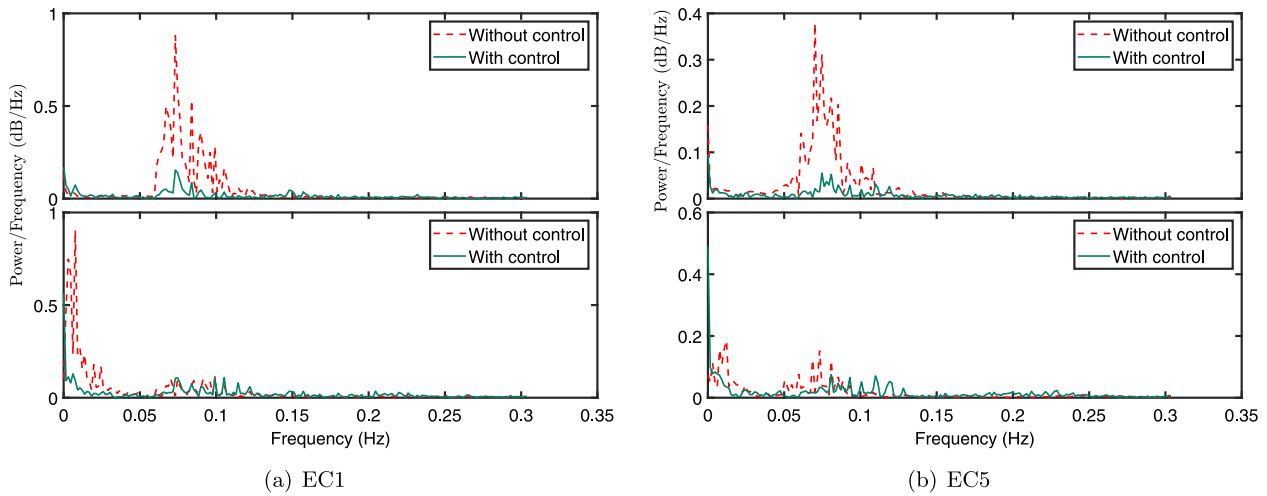
(a) EC1

(b) EC5

Fig. 11. Spectra of the motions at the tower bottom center in EC1 and EC5.
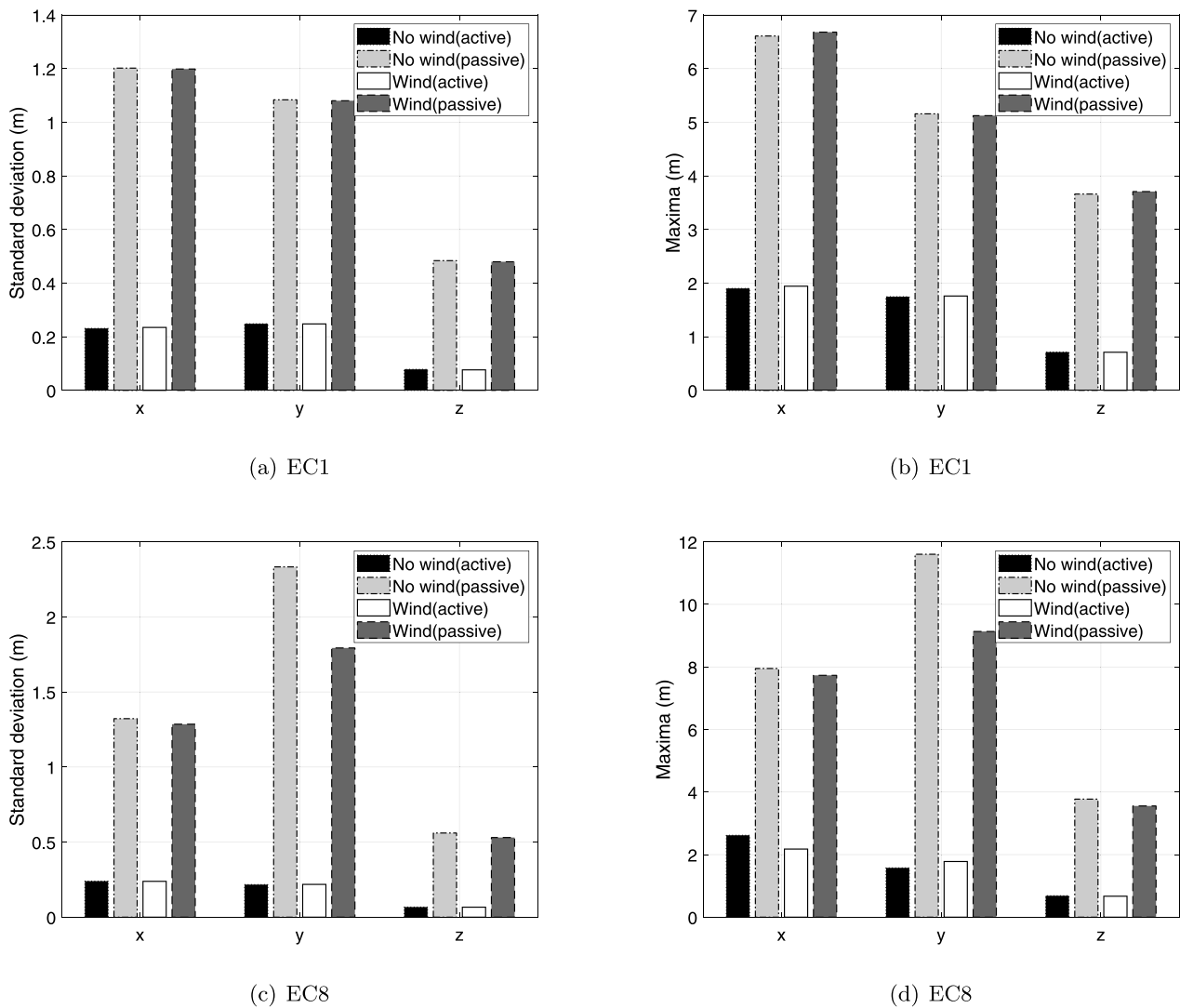

(a) EC1

(b) EC1

(c) EC8

(d) EC8

Fig. 12. The standard derivations and maxima of the displacement at the tower bottom (EC 1 and EC8).

Table 3
Comparison results of the tower bottom position STD and their reductions in the 20 simulations. (Passive: without control; Active: with the proposed control scheme).

EC	x			y			z		
	Passive	Active	Reduction (%)	Passive	Active	Reduction (%)	Passive	Active	Reduction (%)
1	1.2	0.235	80.4	1.08	0.247	77.2	0.485	0.0762	84.3
2	0.159	0.0494	68.9	0.142	0.123	13.1	0.213	0.0428	79.9
3	1.43	0.269	81.1	2.7	0.218	91.9	0.609	0.065	89.3
4	0.28	0.0665	76.2	0.175	0.139	20.8	0.189	0.0426	77.4
5	0.546	0.101	81.6	0.322	0.158	51.0	0.217	0.0434	80.0
6	0.693	0.12	82.8	0.838	0.125	85.1	0.418	0.0554	86.8
7	0.877	0.142	83.8	0.81	0.242	70.1	0.424	0.0774	81.7
8	1.29	0.239	81.5	1.91	0.218	88.6	0.539	0.0655	87.8
9	0.0589	0.0114	80.6	0.0251	0.0167	33.4	0.112	0.014	87.5
10	0.659	0.0895	86.4	0.294	0.0836	71.6	0.222	0.0335	84.9
11	0.699	0.126	81.9	0.496	0.155	68.8	0.271	0.0479	82.3
12	0.206	0.0405	80.3	0.116	0.0554	52.3	0.201	0.0286	85.7
13	0.282	0.0489	82.7	0.0995	0.0634	36.3	0.0836	0.0239	71.5
14	0.312	0.0678	78.3	0.175	0.13	25.4	0.159	0.0393	75.3
15	1.24	0.224	81.8	1.33	0.175	86.8	0.437	0.0539	87.7
16	1.53	0.279	81.8	1.87	0.254	86.4	0.564	0.0736	87.0
17	0.156	0.0415	73.4	0.0658	0.058	12.0	0.155	0.0258	83.3
18	0.541	0.0786	85.5	0.188	0.0605	67.7	0.172	0.0277	83.9
19	0.378	0.0479	87.3	0.157	0.0632	59.7	0.172	0.0323	81.2
20	0.127	0.0144	88.7	0.0787	0.046	41.5	0.15	0.0287	80.8

(a) EC7

(b) EC15
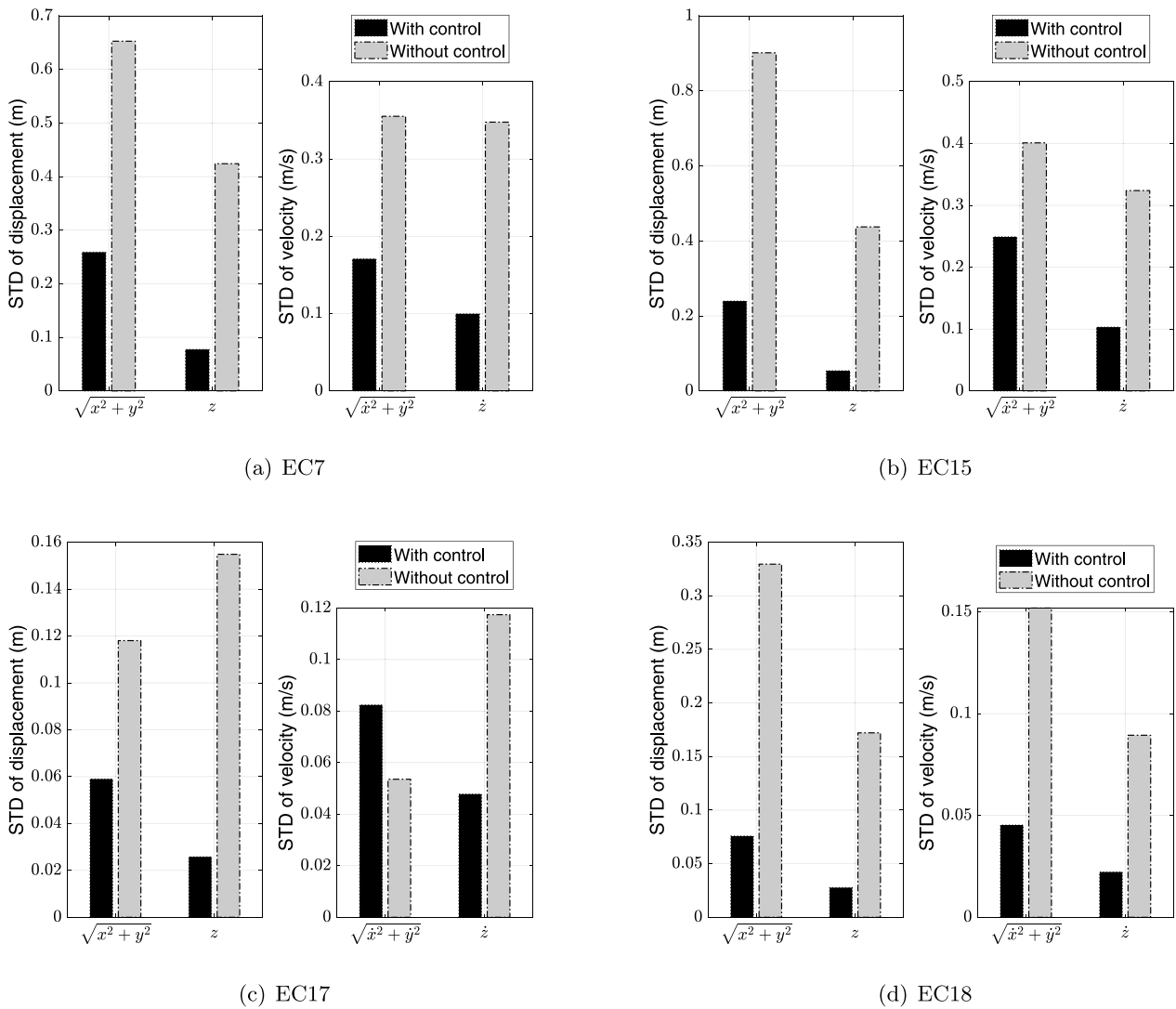

(c) EC17

(d) EC18

Fig. 13. Motions at the tower bottom center in some example ECs.

points may vary due to the small wire elongation, resulting in a small translational oscillation to the preassembly at the connecting points. The resulting small oscillations in rotation introduce large motions at the tower bottom which is far away from the assembly COG.

The geometry and the mass affects the performance of the proposed controller. In the simulations, the influence of wind is not significant due to the high payload mass and small surface area. However, the significance of the wind increases with a larger payload surface area and lower mass. Besides, it is important to note that the control performance is also influenced by the lifting configuration, e.g., the positions of the connection points and base points. A poor arrangement results in inferior performance.

5. Conclusions and future works

In this paper, we manage to design an automatic control solution for general offshore floating lifting operations with a complex-shaped payload and a significant number of lift wires. The main advantage of the proposed control strategy is the model-free characteristic, i.e, without the requirement of state–space equations. It overcomes the design difficulties caused by the configuration complexity and nonlinearities of lift wires. The proposed controller has a simple form, but a satisfied performance, which has been verified by a series of Monte Carlo simulations. In the simulations, the proposed active scheme significantly reduces the payload motion, resulting in more efficient and safe lifting operations. The peak reduction in the spectra of the tower bottom motions reveals that the proposed controller effectively cancel the pendular motion at the payload bottom, i.e., the mating point. If the desired trajectory follows a moving target, it is possible to achieve heave compensation control. Moreover, the scheme consisting of a large number of lift wires has the potential to be extended to the heave lifting problem by sharing the total loads with a large number of wires.

The crane flexibility can introduce additional oscillations to the payload motion. Future studies will investigate the effects of crane stiffness by static and dynamic analysis. The control performance is influenced by the system configuration. The design of optimal lift wire configuration and the arrangement of connecting points are crucial issues to be addressed and evaluated in future publications. Various optimization methods are appliable (Deng et al., 2020a,b).

However, a perfect cancellation is still impossible at the current stage due to the control delay effects, payload geometry, and lift wire elongation. The performance of the controller can be further improved by involving payload motion prediction and considering the real-time wire tension measurements. The feedforward information has the potential to reduce the control delay, resulting a shorter reaction time. Furthermore, time-delayed feedback control is also a promising extension to the proposed strategy. In future papers, time-varying trajectories will be considered to achieve smooth offshore mating operations.

CRediT authorship contribution statement

Zhengru Ren: Methodology, Numerical simulations, Writing - original draft. **Amrit Shankar Verma:** Discussed the results, Revised the manuscript. **Behfar Ataei:** Discussed the results, Revised the manuscript. **Karl Henning Halse:** Discussed the results, Revised the manuscript. **Hans Petter Hildre:** Discussed the results, Revised the manuscript.

Declaration of competing interest

The authors declare that they have no known competing financial interests or personal relationships that could have appeared to influence the work reported in this paper.

Table 4
Notations in the present paper.

$\{b\}$	Payload body-fixed reference frame
d	Damping coefficient of a lift wire
f_c^n	Force acting at the connecting point in $\{n\}$
i	Index of lift wire groups
j	Index of lift wire in the ith group
k	Stiffness of a lift wire
K_i	Positive diagonal matrix
k_p	Control gain
l	Length of a lift wire without elongation
l_d	Desired length of a lift wire
M	Number of lift wire groups
$\{n\}$	Local NED reference frame
N_i	Number of lift wires in the ith group
p^n	Position in $\{n\}$
p_d	Desired position in $\{n\}$
$p_0^n, \ p_0^b$	Positions of concerned point in $\{n\}$ and $\{b\}$
p_b^n	Position of the base point in $\{n\}$
p_c^n	Position of the connecting point in $\{n\}$
p_{cd}^n	Desired position of the connecting point in $\{n\}$
r	Radius of a winch servo motor
R	Rotation matrix
T	Tension acting on a lift wire
u	Control input
$\{v\}$	Vessel body-fixed reference frame
x, y, z	Axes in $\{n\}$
Γ	Coefficient for the lowpass filter
Φ	Vector of Euler angles
ω	Winch rotation speed
Θ_d	Desired orientation

Appendix. Nomenclature

The nomenclature are listed in Table 4.

References

Acero, W.G., Li, L., Gao, Z., Moan, T., 2016. Methodology for assessment of the operational limits and operability of marine operations. Ocean Eng. 125, 308–327.

Adeli, M., Zarabadipour, H., Zarabadi, S.H., Shoorehdeli, M.A., 2011. Anti-swing control for a double-pendulum-type overhead crane via parallel distributed fuzzy LQR controller combined with genetic fuzzy rule set selection. In: 2011 IEEE International Conference on Control System, Computing and Engineering. IEEE, pp. 306–311.

Bak, C., Zahle, F., Bitsche, R., Kim, T., Yde, A., Henriksen, L.C., Hansen, M.H., Blasques, J.P.A.A., Gaunaa, M., Natarajan, A., 2013. The DTU 10-MW reference wind turbine. In: Danish Wind Power Research 2013. Technical Report. Fredericia, Denmark.

Cheng, X., Li, G., Ellefsen, A.L., Chen, S., Hildre, H.P., Zhang, H., 2020. A novel densely connected convolutional neural network for sea-state estimation using ship motion data. IEEE Trans. Instrum. Meas. 69 (9), 5984–5993.

Chu, Y., Æsøy, V., Ehlers, S., Zhang, H., 2015. Integrated multi-domain system modelling and simulation for offshore crane operations. Ship Technol. Res. 62 (1), 36–46.

Deng, W., Xu, J., Gao, X.-Z., Zhao, H., 2020a. An enhanced MSIQDE algorithm with novel multiple strategies for global optimization problems. IEEE Trans. Syst. Man Cybern. Syst..

Deng, W., Xu, J., Zhao, H., Song, Y., 2020b. A novel gate resource allocation method using improved PSO-based QEA. IEEE Trans. Intell. Transp. Syst..

Gustafsson, F., 2010. Statistical Sensor Fusion. Studentlitteratur.

Han, X., Leira, B.J., Sævik, S., 2021. Vessel hydrodynamic model tuning by discrete Bayesian updating using simulated onboard sensor data. Ocean Eng. 220, 108407.

Jiang, Z., Gao, Z., Ren, Z., Li, Y., Duan, L., 2018. A parametric study on the final blade installation process for monopile wind turbines under rough environmental conditions. Eng. Struct. 172, 1042–1056.

Jiang, Z., Hu, W., Dong, W., Gao, Z., Ren, Z., 2017. Structural reliability analysis of wind turbines: a review. Energies 10 (12), 2099.

Kim, G.-H., Pham, P.-T., Ngo, Q.H., Nguyen, Q.C., 2020. Neural network-based robust anti-sway control of an industrial crane subjected to hoisting dynamics and uncertain hydrodynamic forces. Int. J. Control Autom. Syst. 1–9.

Kjelland, M.B., Hansen, M.R., 2015. Offshore wind payload transfer using flexible mobile crane. Model. Identif. Control.

Ku, N.-K., Cha, J.-H., Roh, M.-I., Lee, K.-Y., 2013. A tagline proportional–derivative control method for the anti-swing motion of a heavy load suspended by a floating crane in waves. Proc. Inst. Mech. Eng. M 227 (4), 357–366.

Neupert, J., Mahl, T., Haessig, B., Sawodny, O., Schneider, K., 2008. A heave compensation approach for offshore cranes. In: 2008 American Control Conference. IEEE, pp. 538–543.

Ngo, Q.H., Nguyen, N.P., Nguyen, C.N., Tran, T.H., Ha, Q.P., 2017. Fuzzy sliding mode control of an offshore container crane. Ocean Eng. 140, 125–134.

Niu, H., Lu, Y., Savvaris, A., Tsourdos, A., 2018. An energy-efficient path planning algorithm for unmanned surface vehicles. Ocean Eng. 161, 308–321.

Qian, Y., Fang, Y., Lu, B., 2019. Adaptive robust tracking control for an offshore ship-mounted crane subject to unmatched sea wave disturbances. Mech. Syst. Signal Process. 114, 556–570.

Ren, Z., Han, X., Verma, A.S., Dirdal, J.A., Skjetne, R., 2021a. Sea state estimation based on vessel motion responses: Improved smoothness and robustness using Bézier surface and L1 optimization. Mar. Struct. 76, 102904.

Ren, Z., Jiang, Z., Gao, Z., Skjetne, R., 2018a. Active tugger line force control for single blade installation. Wind Energy 21 (12), 1344–1358.

Ren, Z., Jiang, Z., Skjetne, R., Gao, Z., 2018b. Development and application of a simulator for offshore wind turbine blades installation. Ocean Eng. 166, 380–395.

Ren, Z., Skjetne, R., Gao, Z., 2019a. A crane overload protection controller for blade lifting operation based on model predictive control. Energies 12 (1), 50.

Ren, Z., Skjetne, R., Jiang, Z., Gao, Z., Verma, A.S., 2019b. Integrated GNSS/IMU hub motion estimator for offshore wind turbine blade installation. Mech. Syst. Signal Process. 123, 222–243.

Ren, Z., Skjetne, R., Verma, A.S., Jiang, Z., Gao, Z., Halse, K.H., 2021b. Active heave compensation of floating wind turbine installation using a catamaran construction vessel. Mar. Struct. 75, 102868.

Ren, Z., Verma, A.S., Li, Y., Teuwen, J.J., Jiang, Z., 2021c. Offshore wind turbine operation and maintenance: A state-of-the-art review. Renew. Sustain. Energy Rev. 144, 110886.

Solihin, M.I., Legowo, A., Akmeliawati, R., et al., 2009. Robust PID anti-swing control of automatic gantry crane based on Kharitonov's stability. In: 2009 4th IEEE Conference on Industrial Electronics and Applications. IEEE, pp. 275–280.

Tang, Y., Shi, W., You, J., Michailides, C., 2021. Effects of nonlinear wave loads on large monopile offshore wind turbines with and without ice-breaking cone configuration. J. Mar. Sci. Technol. 26 (1), 37–53.

Velinsky, S., 1985. General nonlinear theory for complex wire rope. Int. J. Mech. Sci. 27 (7–8), 497–507.

Verma, A.S., Jiang, Z., Vedvik, N.P., Gao, Z., Ren, Z., 2019. Impact assessment of a wind turbine blade root during an offshore mating process. Eng. Struct. 180, 205–222.

Vis, I.F., Ursavas, E., 2016. Assessment approaches to logistics for offshore wind energy installation. Sustain. Energy Technol. Assess. 14, 80–91.

Yang, T., Sun, N., Chen, H., Fang, Y., 2019. Neural network-based adaptive antiswing control of an underactuated ship-mounted crane with roll motions and input dead zones. IEEE Tran. Neural Netw. Learn. Syst.

Zekavat, R., Buehrer, R.M., 2011. Handbook of Position Location: Theory, Practice and Advances, vol. 27. John Wiley & Sons.